Reprinted from

Antarctic Meteorite Research, No. 11

A PYROXENE-OLDHAMITE CLAST IN BUSTEE: IGNEOUS AUBRITIC OLDHAMITE AND A MECHANISM FOR THE Ti ENRICHMENT IN AUBRITIC TROILITE

Timothy J. McCoy

National Institute of Polar Research, Tokyo, March 1998

Antarct. Meteorite Res., **11**, 32–48, 1998

A PYROXENE-OLDHAMITE CLAST IN BUSTEE: IGNEOUS AUBRITIC OLDHAMITE AND A MECHANISM FOR THE Ti ENRICHMENT IN AUBRITIC TROILITE

Timothy J. McCoy

Department of Mineral Sciences, MRC 119,
National Museum of Natural History, Smithsonian Institution,
Washington, D.C. 20560, U.S.A.

Abstract: A pyroxene-oldhamite clast in the Bustee aubrite contains major enstatite and minor diopside and forsterite as the silicate host, with abundant (~30 vol%), included 1–5 mm spherules of oldhamite. Within the oldhamite (~5 vol% of the oldhamite) are a variety of phases, including osbornite (TiN), titanoan troilite (17.2–25.2 wt% Ti), heideite (28.7–29.4 wt% Ti), niningerite, daubréelite, forsterite, and Fe metal. This clast represents only the second occurrence of an oldhamite-rich lithology in aubrites. An igneous origin for oldhamite within the Bustee pyroxene-oldhamite clast is suggested by its large size, rounded shapes, presence of included phases formed from multiple, immiscible sulfides, and inclusion of phases unknown from enstatite chondrites. The Bustee clast contains a variety of Ti-rich phases. This work suggests Ti-rich troilite observed in aubrites formed by co-crystallization with or exsolution from Ti-poor sulfides (*e.g.*, oldhamite). In the Bustee case, the undetectably low Ti concentrations in oldhamite and experimental Ti partition coefficient between FeS and CaS approaching infinity support such a suggestion. This mechanism solves the long-standing problem of enriching aubritic troilite in Ti and weakens arguments against a direct derivation of aubrites from known enstatite chondrites.

1. Introduction

Enstatite meteorites are a class of meteorites for which similarities in mineral and oxygen isotopic compositions suggest that a broad group of chondrites (EH, EL), achondrites (aubrites), stony-irons (Mt. Egerton) and irons (Horse Creek) may have related origins (Clayton *et al.*, 1984; Keil, 1989). As such, they provide an ideal opportunity for unraveling the processes of melting and differentiation that changed originally chondritic parent bodies into differentiated asteroids. Research on the origins and relationships between enstatite meteorites has generated a number of important issues. This paper discusses two of these questions.

Can aubrites be derived by melting of known enstatite chondrites? Keil (1969, 1989), and Brett and Keil (1986) marshaled several lines of evidence that aubrites were not derived by melting of known enstatite chondrites on a single parent body. I agree with the conclusion that multiple parent bodies are required based on differences in cosmic-ray exposure ages between enstatite chondrites and aubrites, the lack of aubrite-enstatite chondrite breccias and the implausibly high thermal gradients required for a

single parent body. The issue of whether aubrites could be derived by melting of a known enstatite chondrite is less clear. These authors cited several lines of evidence suggesting that aubrites were derived from an enstatite chondrite-like protolith which differed in several important respects from known enstatite chondrites. The longest standing of these is the problem of Ti abundances in troilite (KEIL, 1969). Enstatite chondrites contain abundant troilite, although that troilite is typically Ti-poor (0.2–0.95 wt% Ti; KEIL, 1969). In contrast, troilite is a minor phase in aubrites, although aubritic troilite exhibits a wide range of Ti concentrations, including grains very enriched in Ti (0.09–16.3 wt% Ti; KEIL, 1969). BRETT and KEIL (1986) and KEIL (1989) argued that there was no known mechanism to enrich Ti in troilite, thus requiring a different precursor for the aubrites from known enstatite chondrites.

Is aubritic oldhamite a crystallization product from the aubritic magma or a relict nebular condensate? Oldhamite is a particularly important mineral in understanding aubrite genesis, as it is the major REE carrier within aubrites (*e.g.*, FLOSS *et al.*, 1990). Similarities between some REE patterns in oldhamite of aubrites and unequilibrated enstatite chondrites (FLOSS and CROZAZ, 1993; CROZAZ and LUNDBERG, 1995) and the extraordinarily high melting temperature of pure CaS (2450–2525°C; VOGEL and HEUMANN, 1941; CHASE *et al.*, 1985) (LODDERS, 1996a,b) have been cited as evidence that most aubritic oldhamite is a relict phase which survived igneous processing on the aubrite parent body. In contrast, textural evidence in an oldhamite-dominated lithology in Norton County (WHEELOCK *et al.*, 1994) and REE patterns in some aubritic oldhamites (FLOSS and CROZAZ, 1993) favors an igneous origin. In addition, partial melting experiments on the Indarch (EH4) enstatite chondrite (DICKINSON and LOFGREN, 1992; FOGEL *et al.*, 1996; MCCOY *et al.*, 1997) do not contain relict oldhamite at temperatures as low as 1200°C, but do contain a multi-component Ca-bearing sulfide melt, suggesting melting of oldhamite at relatively low temperatures. An alternative is an open system model, such as reaction between diopside and a sulfur-rich gas (*e.g.*, FOGEL *et al.*, 1988) to form enstatite and oldhamite. However, this reaction would also liberate large amounts of SiO_2, a phase not found in abundance in aubrites, suggesting this is not a viable mechanism. A full discussion of the intricacies of REE partitioning in oldhamite are beyond the scope of this paper, but contrasting discussions of experimental REE partitioning in oldhamite are given by LODDERS (1996a,b) and DICKINSON and MCCOY (1997).

My petrologic study of a pyroxene-oldhamite clast in Bustee and an experiment on Ti partitioning between CaS and FeS provides important insights into these questions and suggests that their solutions are linked.

2. Previous Work

Bustee fell on December 2, 1852, in India and was first described by STORY-MASKELYNE (1870). The most remarkable feature of Bustee is a pyroxene-oldhamite clast ~ 4 cm in diameter from which STORY-MASKELYNE (1870) described two new minerals. The first of these is oldhamite (CaS), which occurs as abundant 1–5 mm spheres within the clast. Osbornite was also described from this clast, although the available material was too rare and the available analytical techniques too primitive to accurately determine its composition. STORY-MASKELYNE (1870) thought it might be an oxysulfide

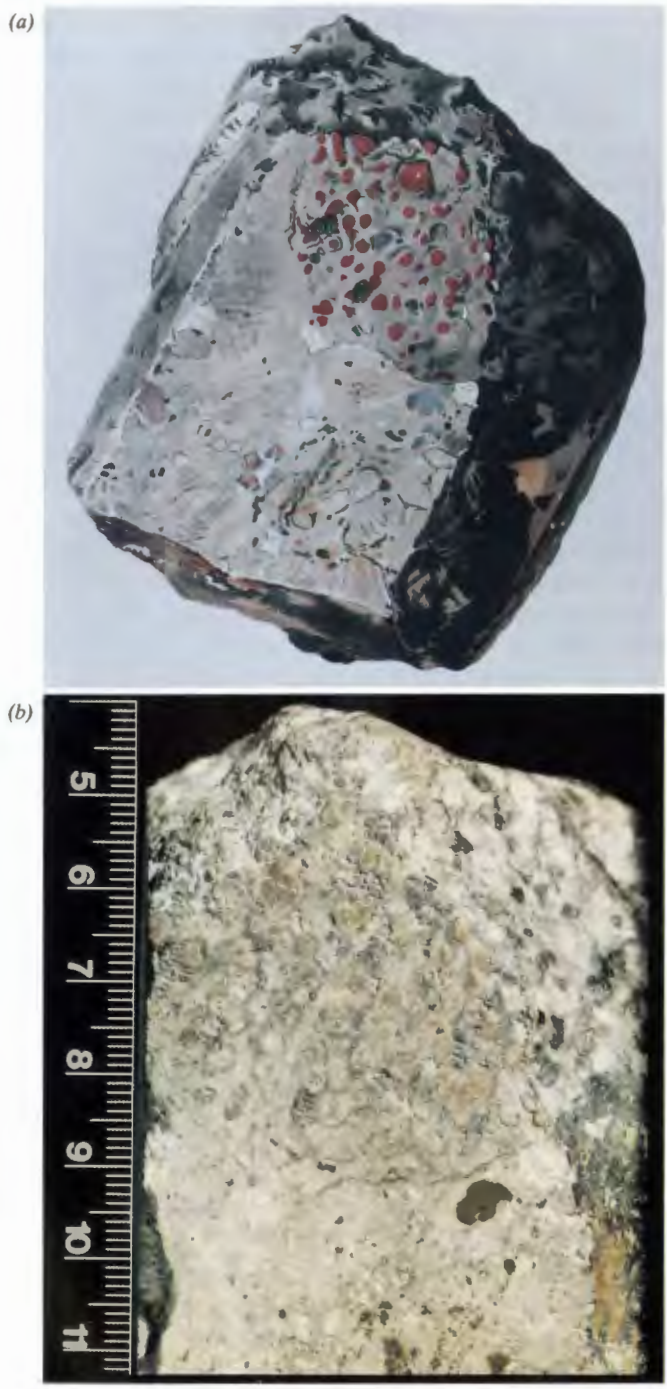

Fig. 1. The main mass of the Bustee aubrite illustrating the pyroxene-oldhamite clast. (a) Colored lithograph from Flight *(1875, 1887). The pyroxene-oldhamite clast contains abundant 1–5 mm sized chestnut brown oldhamites. (b) Photograph of the main mass of Bustee showing the same face illustrated by* Flight *(1875, 1887). The oldhamite spherules appear pink. Scale bar is in cm.*

of calcium, titanium, and/or zirconium. FLIGHT (1875, 1887) published a condensed version of STORY-MASKELYNE's (1870) report, but included a remarkable colored lithograph of the main mass of Bustee (Fig. 1a). In this image, the pyroxene-oldhamite clast with its multi-mm sized chestnut brown oldhamites are apparent. The Natural History Museum in London has maintained the original surface illustrated by FLIGHT (1875, 1887) intact to this day (Fig. 1b). The large, pink oldhamites are clearly visible within the pyroxene-oldhamite clast. BANNISTER (1941) reanalyzed osbornite and determined it to be titanium nitride (TiN). KURAT *et al.* (1992), in abstract form, provided the only modern study of the Bustee pyroxene-oldhamite clast. The major focus of this work was analysis of rare earth elements and isotopic compositions of the phases in the pyroxene-oldhamite clast, although they did note the occurrence of metal (Si- and Cr-bearing), heideite, osbornite and a few other rare sulfides. The REE pattern they observed in oldhamite was flat at 40–100×CI with a positive europium anomaly. The flat patterns observed by these authors in oldhamite, osbornite, diopside and enstatite suggested to them that the minerals of the pyroxene-oldhamite clast formed by condensation, not by crystal-chemically controlled partitioning from a melt.

3. Samples and Techniques

I studied polished thin section BM 32100,P5116 of the Bustee pyroxene-oldhamite clast, which was generously provided by Dr. Monica GRADY of The Natural History Museum, London, United Kingdom. This thin section was studied in transmitted and reflected light. Elemental mapping and quantitative analyses were conducted using a Cameca SX-100 electron microprobe at NASA/Johnson Space Center, Houston, Texas, USA. Automated area analysis of selected elemental maps was utilized to obtain approximate modal abundances of phases in the pyroxene-oldhamite clast. Quantitative analyses were conducted using a 15 nA beam current, 20 keV accelerating voltage and a fully-focused beam. Well-known natural and synthetic standards were used and data were corrected using the manufacturer-supplied PAP ZAF program. Typical detection limits in metal and sulfides were 0.02 wt% for Ti, Mg, Ca, Cr, Fe, Na, Zn and S; 0.03 wt% for Mn; and 0.06 wt% for Ni and Co. Detection limits in silicates were 0.02 wt% for SiO_2, Al_2O_3, MgO, Na_2O and CaO and 0.04 wt% for FeO.

In order to better understand the petrogenesis of aubritic sulfides, the partitioning of Ti between FeS and CaS was investigated experimentally. A mixture of 100 mg of FeS_2, 46.7 mg of CaO and 5 mg of TiO_2 was ground in an agate mortar, producing a composition with an atomic Fe:Ca ratio of 1:1 and ~2.2 wt% Ti in the bulk. Approximately 40 mg of this mixture was placed in a graphite crucible. The graphite crucible was placed in a silica tube and an alumina crucible with Cr metal was placed above the graphite crucible as an oxygen getter to produce the low oxygen fugacities required for CaS formation ($(\log fO_2)_{Cr\text{-}Cr_2O_3} = -16.3$ at 1300°C or ~4 log units below iron-wüstite). The silica tube was evacuated and sealed. This mixture was placed in a Deltech vertical gas-mixing furnace at Johnson Space Center and held at 1300°C for 24 hours. The oxygen fugacity within the furnace was held near the iron-wüstite buffer to improve tube stability. At the conclusion of the experiment, the silica tube with the sample was quenched in flowing air. No water was used during quenching or section preparation to

avoid alteration of CaS. The sample was examined in reflected light and analyzed using a JEOL JXA-8900R electron microprobe at the National Museum of Natural History, Smithsonian Institution, Washington, DC, USA, using a 15 nA beam current, 20 keV accelerating voltage and a fully-focused beam. Well-known natural and synthetic standards were used and the data were corrected using a ZAF program.

4. Results

4.1. Petrography of the Bustee clast

Silicates comprise ~70% of the pyroxene-oldhamite clast. Enstatite contains undetectably low FeO concentrations (Table 1) and is the dominant silicate phase. Individual enstatite grains range from 0.5 to 5 mm in maximum dimension. Enstatite-enstatite grain boundaries range from smooth boundaries with occasional 120° triple junctions to irregular, ragged intergrowths more typical of aubrites. Blebby diopsides are found both within individual enstatite grains and on enstatite-enstatite grain boundaries (Fig.

Table 1. Average silicate compositions (wt%) in the Bustee pyroxene-oldhamite clast.

	Enstatite	Diopside	Forsterite
SiO_2	59.1	55.0	42.4
	0.38	*0.39*	*0.24*
TiO_2	0.09	0.55	b.d.
	0.02	*0.03*	
Al_2O_3	0.07	0.17	b.d.
	0.01	*0.02*	
MgO	39.9	20.4	57.2
	0.15	*0.26*	*0.23*
CaO	0.37	23.6	b.d.
	0.05	*0.31*	
Na_2O	b.d.	0.14	b.d.
		0.02	
Total	99.53	99.86	99.6
N	9	10	10
	Molar Proportions		
Si	0.99	0.99	1.00
Ti	-	0.01	-
Al	-	-	-
Mg	1.00	0.55	2.01
Ca	0.01	0.45	-
Na	-	-	-
O	3.00	3.00	4.00

b.d. = below detection limits; N = Number of analyses. Italicized figures are 1σ of analytical variability. Cr_2O_3, FeO, MnO and K_2O were below detection limits in all phases.

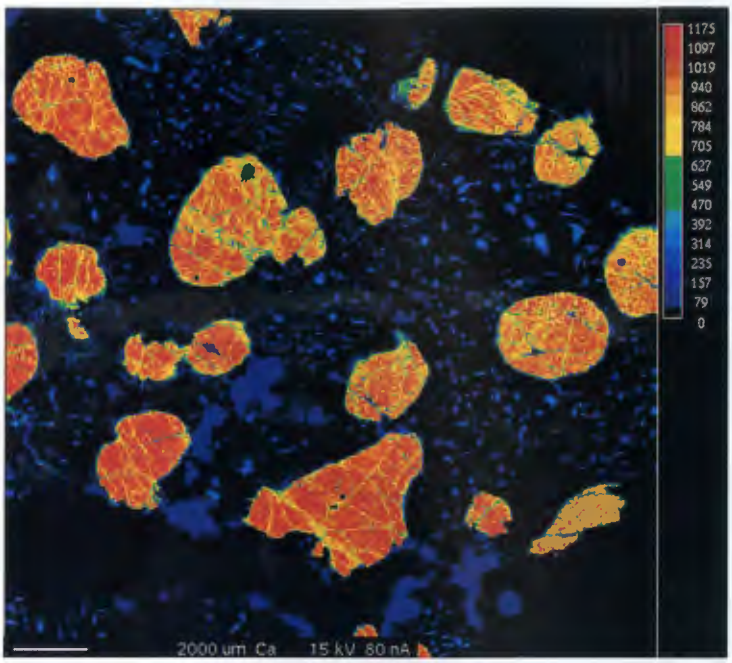

Fig. 2. Calcium X-ray map of the pyroxene-oldhamite clast in Bustee. Scale bar = 2 mm. Oldhamite spherules appear in orange, but contain yellow to green weathering area along fractures. The oldhamite spherules are rounded to irregularly shaped and are sometimes sheared by later shock. Blebby diopsides within the silicate host appear blue.

2). These diopsides range from 50 μm to 1 mm in maximum dimension. It is interesting that both enstatite and diopside contain significant concentrations of TiO_2 (0.09 and 0.55 wt%, respectively). Forsterites up to 300 μm in maximum dimension are occasionally observed in association with the oldhamite spheres. Despite a careful search, including elemental mapping, no plagioclase was observed. KURAT *et al.* (1992) asserted that STORY-MASKELYNE (1870) observed plagioclase. In fact, STORY-MASKELYNE (1870, p. 207) specifically notes the absence of alumina and, hence, any feldspathic component. Rare osbornites up to 20 μm in maximum dimension are also observed within the silicates. They appear to be randomly distributed.

The most striking feature of the pyroxene-oldhamite clast is the presence of large (1–5 mm) oldhamite spherules (Figs. 1a,b, 2). These oldhamite spherules are approximately evenly distributed throughout the clast and comprise ~30% by volume. The oldhamites range in shape from rounded to irregular (Fig. 2). The spherules exhibit a pinkish-red color in transmitted light, are isotropic, and exhibit cubic cleavage typical of oldhamite. Shearing by later shock is a fairly common feature within the oldhamite spherules and some of these spherules have hemispheres offset along a planar fracture (Fig. 2, 3a). The average composition for the oldhamite within the clast is given in

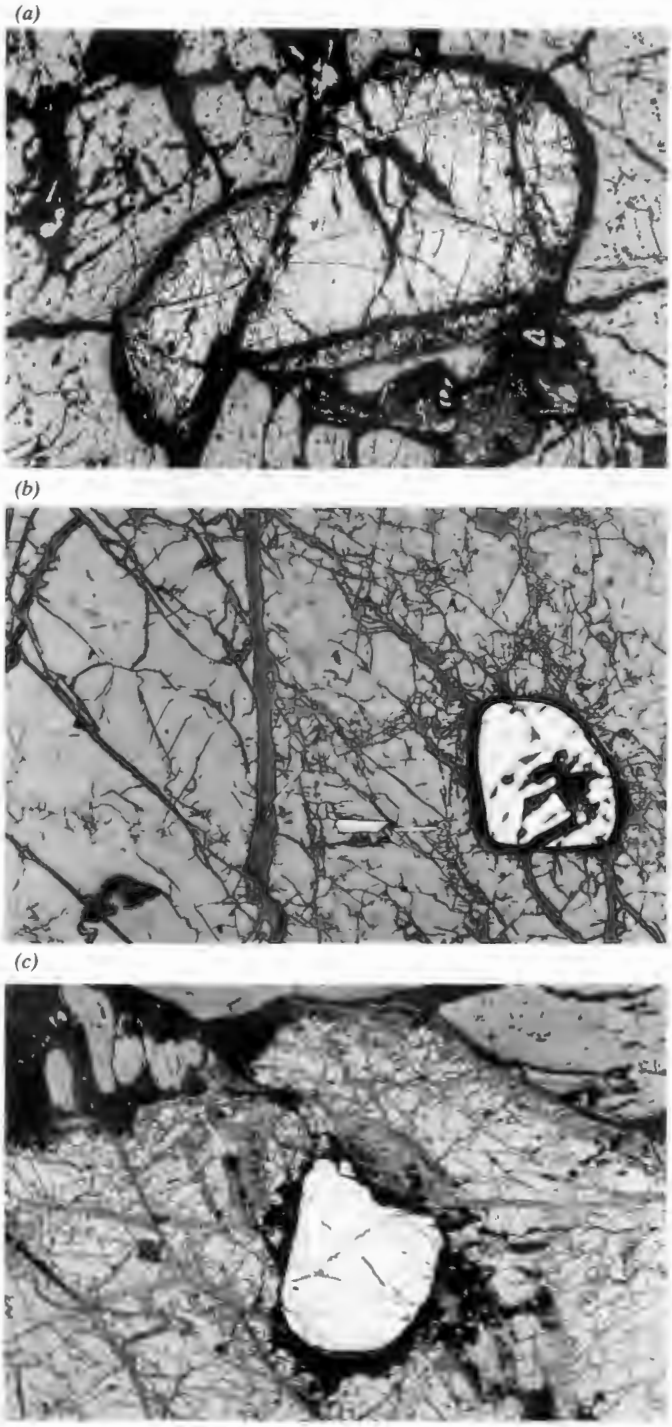

Fig. 3. Photomicrographs of oldhamite and included phases in the Bustee pyroxene-oldhamite clast. (a) A rounded oldhamite spherule which was sheared by a later shock event. Field of view = 2.6 mm. (b) Large (120 μm) isolated osbornite within host oldhamite. Within the oldhamite, lath-shaped troilite oriented along the crystallographic axes of the host oldhamite can be seen. It appears that this troilite formed by exsolution from the host oldhamite. Field of view = 650 μm. (c) Large (300 μm), rounded to subhedral, isolated titanoan troilite within oldhamite host. The oldhamite-silicate boundary is visible at the top of the image. This grain of troilite contains 23.3 wt% titanium. It likely represents an immiscible Fe-rich sulfide melt which crystallized slightly after the Ca-rich sulfide melt in which it is enclosed. Field of view = 1.3 mm.

Table 2. The composition corresponds to a formula of $(Ca_{0.96}Mg_{0.03}Mn_{0.01})S$. Microprobe totals for oldhamite in this work were systematically low (~96 wt%). Low totals for oldhamite analyses have been reported by other authors (*e.g.*, WHEELOCK *et al.*, 1994; DICKINSON and MCCOY, 1997) and likely reflect the very rapid weathering of this highly-reduced mineral.

The large oldhamite spherules contain a variety of included phases, which comprise ~5 vol% of the oldhamite (~1 vol% of the whole rock). These are titanoan troilite, osbornite, niningerite, heideite, daubréelite, metal, and forsterite. I will discuss each of

Table 2. Average compositions (wt%) and atomic proportions for oldhamite, heideite, daubréelite, niningerite and metal and representative analyses for titanoan troilite in the Bustee pyroxene-oldhamite clast.

	Oldhamite	Titanoan Troilite			Heideite	Daubréelite	Niningerite	Metal
Ca	51.5	0.35	b.d.	0.60	0.39	0.18	0.51	n.d.
	0.17				*0.01*	*0.14*	*0.10*	
S	43.1	40.4	42.7	43.4	44.2	44.1	50.1	n.d.
	0.26				*0.62*	*0.14*	*0.79*	
Fe	b.d.	39.3	31.6	29.7	24.5	18.0	6.87	98.9
					0.59	*0.16*	*1.15*	*0.77*
Ti	b.d.	17.2	23.3	25.2	29.1	0.22	b.d.	n.d.
					0.52	*0.08*		
Cr	b.d.	2.15	2.64	1.71	1.80	35.8	b.d.	0.28
					0.12	*0.23*		*0.25*
Ni	b.d.	b.d.	0.18	b.d.	b.d.	b.d.	b.d.	0.29
								0.11
Mn	0.47	b.d.	b.d.	b.d.	b.d.	b.d.	13.3	n.d.
	0.02						*1.10*	
Mg	1.00	b.d.	b.d.	b.d.	b.d.	b.d.	29.1	n.d.
	0.08						*1.24*	
Co	n.d.	n.d.	n.d.	n.d.	n.d.	n.d.	n.d.	b.d.
Total	96.07	99.40	100.42	100.61	99.99	98.3	99.88	99.52
N	6	1	1	1	2	4	6	7
				Atomic Proportions				
Ca	0.96	0.01	-	0.01	0.03	0.01	0.01	-
S	1.00	1.00	1.00	1.00	4.00	4.00	1.00	-
Fe	-	0.56	0.43	0.39	1.27	0.94	0.08	0.99
Ti	-	0.28	0.37	0.39	1.76	0.01	-	-
Cr	-	0.03	0.04	0.02	0.10	2.00	-	-
Ni	-	-	-	-	-	-	-	<0.01
Mn	0.01	-	-	-	-	-	0.16	<0.01
Mg	0.03	-	-	-	-	-	0.77	-
Co	-	-	-	-	-	-	-	-

b.d. = below detection limits; n.d. = not determined; N = Number of points analyzed.
Figures in italics are 1σ of analytical variability for N points.
Na and Zn were below detection in all sulfides analyzed.
Si and P were both below detection in metal.

these in turn. The oldhamite-pyroxene clast is the type specimen for osbornite and it occurs as individual grains up to 120 μm in diameter (Fig. 3b). These grains are typically rounded or subhedral. I did not quantitatively analyze osbornite, but it was easily recognized on the basis of strong Ti and N signals during elemental mapping and its distinctive gold-colored reflectivity. Stoichiometric TiN would contain 77.4 wt% Ti and 22.6 wt% N. In one case, I observed osbornite grains of a few microns in size within daubréelite.

Titanoan troilite is widespread in the oldhamite spherules and is the most common phase included within the oldhamite. Troilite was not observed within the silicate host in the Bustee pyroxene-oldhamite clast. Within the oldhamite spherules, titanoan troilite is one of several phases which occur either as isolated grains or as compound particles consisting of one or more of titanoan troilite, metal, daubréelite, heideite and niningerite. Titanoan troilite occurs as isolated, rounded to semi-equant grains up to 300 μm in diameter (Fig. 3c). It also occurs as laths oriented along the crystallographic axes of the host oldhamite (Fig. 3b), suggesting formation by exsolution. Representative analyses of titanoan troilite are given in Table 2. Titanium concentrations of troilite within the pyroxene-oldhamite clast range from 17.2–25.2 wt%. This corresponds to formulas of $(Fe_{0.56}Ti_{0.28}Cr_{0.03})S$ to $(Fe_{0.39}Ti_{0.39}Cr_{0.02})S$. Note that charge balance requires Ti^{3+} and, hence, the descriptor titanoan (Nickel and Mandarino, 1987). Ranges of Ti concentrations of troilites in individual oldhamite spherules ($\leq$2.3 wt%) are considerably smaller than that for the clast as a whole (8 wt%). As a whole, Bustee contains troilite with a very broad range of titanium concentrations from 0.2 wt% to 25.2 wt% (Keil and Brett, 1974; this work). Figure 4 illustrates the compositions of titanoan troilite and heideite in Bustee on a plot of the hypothetical components S, (Fe,Cr)S and TiS. As can be clearly seen, Bustee troilites exhibit a much broader range of Ti concen-

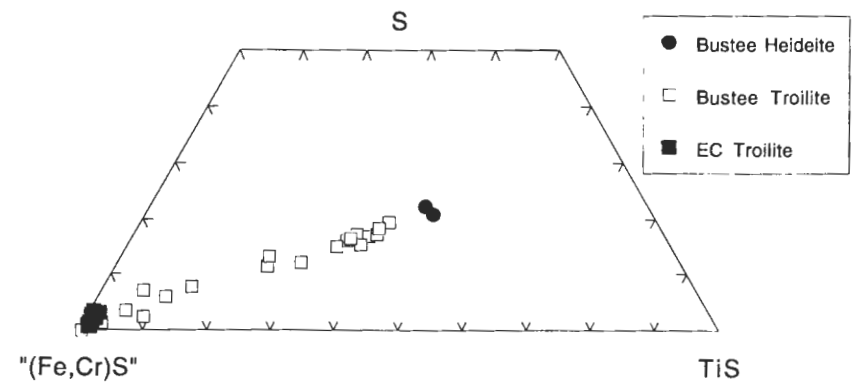

Fig. 4. Compositions of titanoan troilite and heideite in Bustee (mole% of the hypothetical components S, (Fe,Cr)S and TiS). Bustee contains troilites with a very broad range of titanium concentrations from 0.2 wt% to 25.2 wt% (Keil and Brett, 1974; this work), a much broader range than observed in enstatite chondrite (EC) troilites (Keil, 1968). These Bustee troilite compositions trend towards Ti-rich sulfide heideite, suggesting solid solution between troilite and heideite.

trations than observed in enstatite chondrite (EC) troilites (KEIL, 1968). These Bustee troilite compositions trend towards the Ti-rich sulfide heideite, suggesting that troilite and heideite may represent end-members of a continuous solid-solution series. Alternatively, although intergrowths of these two phases were not observed in the optical or scanning electron microscope, I cannot unequivocally eliminate the possibility that troilite and heideite are intergrown on a sub-micron scale. The detailed TEM and/or XRF study of this material needed to resolve this issue was beyond the scope of this study.

Bustee is the type specimen for heideite (KEIL and BRETT, 1974), although these authors did not examine the pyroxene-oldhamite clast. Two grains of heideite were found in one of the oldhamite spherules. KURAT *et al.* (1992) also cited the presence of heideite in the pyroxene-oldhamite clast of Bustee. The average composition is given in Table 2, corresponding to a formula of $(Fe^{2+}_{1.03}Cr^{2+}_{0.10}Ca^{2+}_{0.03})(Ti^{3+}_{1.76}Fe^{2+}_{0.24})S_4$. Heideite in the Bustee pyroxene-oldhamite clast is very rich in titanium, containing 28.7–29.4 wt% Ti.

Daubréelite was observed in several of the oldhamite spherules. Its average composition (Table 2) corresponds to a formula of $(Fe_{0.94}Ca_{0.01}Ti_{0.01})Cr_{2.00}S_4$. It was found intergrown with a number of other sulfides, as well as metal.

Niningerite was observed in several of the oldhamite spherules. Its average composition (Table 2) corresponds to a formula of $(Mg_{0.77}Mn_{0.15}Fe_{0.08}Ca_{0.01})S$. Niningerite occurs as both isolated grains and compound grains associated with titanoan troilite and metal. Although sometimes associated with lath-like titanoan troilite grains, its shape is typically irregular, yielding little clues to its origin (*e.g.*, crystallization from a melt *vs.* solid-state exsolution). Niningerite is a relatively rare phase in aubrites, although an Fe-dominated niningerite was observed by KEIL *et al.* (1989) in Shallowater.

Metal has been identified both within and at the edges of the oldhamite spherules. Quantitative analyses (Table 2) reveals that this metal contains significant and variable Cr concentrations, minor (0.1–0.4 wt%) Ni concentrations and is essentially Si free. I could not confirm the finding of KURAT *et al.* (1992) that the clast contains Si-bearing metal. The low Ni concentration of the metal suggests that it may have formed by reduction of FeO to Fe metal. The source of this FeO is uncertain, although it may have been minute amounts of FeO in adjacent enstatite.

A single grain of forsterite was found entirely contained within an oldhamite spherule, at least in the plane of the thin section. The forsterite grain is lath-shaped (5×100 μm) and is found ~400 μm from the edge of the oldhamite spherule. It does not appear to be oriented along the crystallographic axes of the host oldhamite. Excluding 0.39 wt% CaO probably resulting from beam overlap with the enclosing oldhamite, the grain was stoichiometrically pure Mg_2SiO_4.

4.2. Experimental study of Ti partitioning between FeS and CaS

I have conducted a single experiment on the partitioning of Ti between FeS and CaS (see Section 3). It is important to emphasize that this single experiment should be considered as a reconnaissance of Ti partitioning in this system. A more complete study will be needed to fully evaluate important issues such as reproducibility, equilibrium, temperature dependence and Henry's Law behavior. This experiment produced CaS

spherules ~100 μm in diameter with an interstitial intergrowth of FeS and Fe metal, confirming the immiscibility between FeS and CaS reported by previous workers. Occasionally, larger Fe metal spheres are also present in the charge. Locally, it appears that contamination with silicates occurred and I found a Ca,Ti,S,Si-phase. I do not believe that the presence of this phase dramatically altered the partitioning of Ti between co-existing FeS and CaS, particularly since this Ca,Ti,S,Si-phase is not widespread. This experiment confirms that Ti is strongly partitioned into FeS during co-crystallization with CaS. The average composition of 5 analyses of the FeS is 52.6 wt% Fe, 37.6 wt% S, 7.24 wt% Ti and 0.22 wt% Ca. Titanium in the FeS ranged between 6.2–7.7 wt% Ti. Co-existing CaS has an average composition (5 analyses) of 54.1 wt% Ca, 42.4 wt% S, 1.32 wt% Fe and Ti below detection limits (<0.02 wt%). A partition coefficient for Ti between FeS and CaS ($(D_{Ti})_{FeS/CaS}$) would approach infinity.

5. Discussion

5.1. A second oldhamite-rich lithology from aubrites

Although oldhamite is ubiquitous in aubrites, it typically occurs as grains less than 500 μm in size scattered throughout the brecciated matrix of aubrites (Floss and Crozaz, 1993) and comprises only a fraction of a volume percent of the whole rock (Watters and Prinz, 1979). Oldhamite-rich lithologies are, however, known from aubrites. Wheelock *et al.* (1994) described an oldhamite-dominated lithology from the Norton County aubrite. This lithology, represented by a series of clasts, consists of large (up to 2 cm) single crystals of oldhamite. The oldhamite (86.6 vol% of the sulfides) contains inclusions of ferromagnesian alabandite (9.7%), troilite (2.15%), daubréelite (0.85%), caswellsilverite (0.65%) and Fe,Ni metal (0.10%). The silicate portion of the lithology is primarily FeO-free forsterite, with some enstatite and plagioclase. No modal analyses of the silicates was reported.

An oldhamite-enriched shock melt vein has also been observed in the Jajh deh Kot Lalu enstatite chondrite (Rubin *et al.*, 1997). This ~2×16 mm chondrule-free vein contains 6.7 wt% oldhamite. Oldhamite grains range up to 100 μm in maximum dimension. Most are anhedral, although a few are subhedral. Enstatite, plagioclase and minor kamacite are also present.

The pyroxene-oldhamite clast in Bustee represents a second oldhamite-rich lithology from aubrites. While the Bustee and Norton County lithologies are similar in containing abundant, large oldhamite crystals, it is clear that they sample two distinct lithologies. Unlike the Norton County oldhamite-dominated lithology, the Bustee pyroxene-oldhamite clast contains titanoan troilite as the dominant inclusion phase with oldhamite. In addition, the Bustee oldhamites contain heideite, niningerite and osbornite and lack ferromagnesian alabandite and caswellsilverite. Finally, the Norton County lithology contains dominantly forsterite in its silicate portion, while forsterite is a very minor phase in the Bustee pyroxene-oldhamite clast and plagioclase is absent from this lithology. Thus, aubrites are known to contain at least two distinct oldhamite-rich lithologies. Continued searches of aubrite clasts would undoubtedly reveal more oldhamite-rich lithologies.

5.2. Igneous aubritic oldhamite

The origin of aubritic oldhamite is a topic of considerable debate, as discussed earlier. In this specific case, several lines of evidence can be advanced that the pyroxene-oldhamite lithology in Bustee formed as a result of igneous processes on the aubrite parent body. I apply these arguments specifically to the Bustee clast, although many of these same arguments were marshaled by WHEELOCK *et al.* (1994) in the case of the oldhamite-dominated lithology in Norton County. These are:

1) The ragged intergrowths of some enstatite grains is suggestive of intergrowth during co-crystallization. The blebby diopside found on grain boundaries and within single enstatite grains may have co-crystallized with the enstatite or may have exsolved later.
2) The large size (up to 5 mm) and rounded shapes of the oldhamite grains (Fig. 2) is entirely consistent with crystallization of an immiscible sulfide melt within a silicate melt. In this case, the silicate phase dominates and, hence, the sulfide melt formed rounded blebs within the silicate. It is difficult to reconcile such large crystal sizes with condensation in the solar nebula. An alternative explanation was offered by LODDERS (1996b), who argues that such large grains form by aggregation of smaller relict oldhamite grains and subsequent annealing.
3) The presence of large, rounded to subhedral troilite grains within the oldhamite spherules is entirely consistent with an igneous history, but inconsistent with nebular condensation. Immiscibility in the Fe-Ca-Mg-S system has been demonstrated by several workers (*e.g.*, DICKINSON and MCCOY, 1997) at temperatures as low as 1200°C. Melts in this system separate into two immiscible sulfide melts, one Fe-rich and one Ca-Mg-rich. Thus, the presence of minor quantities of rounded to subhedral troilite (FeS) within oldhamite (CaS) (Fig. 3c) is strongly suggestive that the FeS formed as immiscible sulfide melt blebs within a CaS melt. In contrast, the observed phase assemblage and distribution are inconsistent with a condensation origin. For example, FeS occurs within CaS. However, FeS should condense at 700 K (GROSSMAN, 1971) while CaS condenses at 1379 K at 10^{-3} bars (LODDERS and FEGLEY, 1992). A phase with a low condensation temperature (FeS) should not occur inside one with a high condensation temperature (CaS). Thus, it seems highly implausible that the oldhamite formed by condensation.
4) An argument unique to the Bustee clast and perhaps the most compelling evidence against a relict origin concerns the phase assemblage contained within the oldhamite spherules. In particular, several of the phases (*e.g.*, Ti-rich troilite, heideite) are simply unknown from enstatite chondrites. Further, although osbornite is known from enstatite chondrites, it occurs in the Bustee clast as grains an order of magnitude larger than any seen in enstatite chondrites. In the absence of these phases from enstatite chondrites, it is very difficult to imagine that the Bustee oldhamite is a relict from an enstatite chondrite which escaped melting on the aubrite parent body.

I envision a history for the Bustee clast in which a complex silicate-sulfide melt formed on the aubrite parent body. Exactly how this melt formed is unclear. FOGEL *et al.* (1996) have argued that S dissolved in silicate melts at low oxygen fugacities will com-

plex with Ca and, upon cooling, an immiscible CaS melt will form. A full discussion of this mechanism is beyond the scope of this paper. Experiments by Fogel *et al.* (1996) and McCoy *et al.* (1997) suggest that a series of oxidation/reduction (*e.g.*, $CaO+{}^1/_2 S_2 \rightarrow CaS+{}^1/_2O_2$) and exchange reactions (*e.g.*, $SiO_2 \rightarrow Si + {}^1/_2O_2$) are involved in this process and the reader is referred to these works for further details. The oldhamite spherules in the Bustee clast may have formed by this mechanism. It seems likely that the immiscible CaS melt formed upon cooling would have occurred as small droplets which coalesced to form the mm-sized spherules in the Bustee clast. Evidence of this process may be found in the occurrence of a dumbbell shaped oldhamite particle (Fig. 2) which may represent coalescing immiscible CaS melts. Unlike other sulfides, a CaS melt may not readily separate from the silicate melt. Dickinson and McCoy (1997) produced CaS melts which did not readily separate from the silicates in their experimental charges. Further, Rubin *et al.* (1997) calculated similar densities for crystalline CaS and molten enstatite chondrite silicates, suggesting that separation would not occur after oldhamite crystallization in a silicate melt. The silicate melt was the dominant component and a calcium sulfide melt formed immiscible blebs which themselves included blebs of immiscible iron sulfide melts. It is difficult to deduce the relative crystallization order of the silicates, Ca-rich sulfide and Fe-rich sulfide. Crystallization may have occurred essentially contemporaneously, although the semi-equant shapes of some troilites suggests that crystallization of the Fe-rich sulfide melt may have occurred after the beginning of CaS crystallization. Upon cooling, several other sulfides, including daubréelite and the lath-shaped troilites, exsolved from the host oldhamite. A subsequent shock event sheared and deformed the oldhamite spherules.

This interpretation of the history of the Bustee pyroxene-oldhamite clast differs dramatically from that of Kurat *et al.* (1992), which was based primarily on the REE patterns in the clast phases. These authors inferred a condensation sequence of osbornite-oldhamite-pigeonite-enstatite. A full discussion of how the REE patterns in the Bustee pyroxene-oldhamite clast could have been established during igneous crystallization is beyond the scope of this paper. Dickinson and McCoy (1997) have discussed at length and in a general sense the complex array of processes which determine the REE abundances and patterns within crystallizing oldhamite in an aubritic magma.

5.3. The Ti in troilite problem

A remarkable feature of the pyroxene-oldhamite clast in Bustee is its Ti-rich nature. This clast contains significant quantities of titanoan troilite (17.2–25.2 wt% Ti) and osbornite (ideally 77.4 wt% Ti), as well as rare grains of heideite (28.7–29.4 wt% Ti). Both enstatite and diopside within the pyroxene-oldhamite clast are also anomalously rich in Ti. The presence of such Ti enrichment within this clast suggests that it may hold the key to the solution of the long-standing problem of how to enrich aubritic troilite in Ti compared to troilite in enstatite chondrites.

Several solutions to the Ti in troilite problem have been previously proposed and it is worth discussing these briefly. Several authors (Keil, 1969; Fogel *et al.*, 1988) have suggested that differences in melting temperature and/or density between Ti-rich and Ti-poor troilite could result in fractionation of these two components during melting of an

enstatite chondrite-like protolith. Indeed, there are substantial differences in these properties between FeS (1195°C; ~4.7 g/cm^3) and TiS (1927°C; ~4.2 g/cm^3) (KEIL, 1969; FOGEL *et al.*, 1988). However, enstatite chondrites exhibit a relatively small range of Ti concentrations in troilite (0.2–0.95 wt% Ti; KEIL, 1969). The differences in density and melting temperature between these troilites would be essentially insignificant. KEIL (1969) considered and rejected immiscibility in the Fe-Ti-S system, since experiments by R. BRETT (reported in KEIL, 1969) showed no immiscibility in this system at 1375°C. CASANOVA (1992) suggested that melting of osbornite (TiN) and incorporation of Ti bound in osbornite in enstatite chondrites could produce Ti-rich troilite in aubrites. This hypothesis seems unworkable since in Bustee I find co-existing osbornite and the most Ti-rich troilite yet observed in aubrites (25.2 wt% Ti). Very recently, FOGEL (1997) has proposed that incorporation of sulfur into silicate melts upon melting of enstatite chondrites can produce the observed Ti enrichment. In this model, the parental material is an enstatite chondrite with Fe,Ni metal and titanium-bearing troilite. As this material melts, S moves into the silicate melt, combining with Ca, as noted earlier. This movement of S into the silicate melt enriches the residual Fe,Ni-FeS melt in Fe and Ti. While the Fe forms metal, the Ti is incorporated into the Fe-sulfide component, enriching it in Ti. This model may explain a part of the enrichment in Ti concentrations in aubritic sulfides. However, experimental melting of the Indarch (EH4) enstatite chondrite (MCCOY *et al.*, 1997), in which substantial S (6.0 wt% at 1425°C) is incorporated into the silicate melt, produced co-existing sulfide melts with <1 wt% Ti. A possible explanation for the lack of Ti enrichment in co-existing sulfides is the incorporation of Ti into the silicate melt. MCCOY *et al.* (1997) observed TiO_2 concentrations in the silicate melt increasing with S concentrations and temperature. The experiments of MCCOY *et al.* (1997) are preliminary and clearly more work is needed to trace the partitioning of Ti during the melting of enstatite chondrites.

Despite the inability to determine the mechanism for enriching troilite in Ti, it seems clear that such a mechanism must exist. In the absence of such a mechanism, one must postulate a chondritic precursor which contained troilite with a broad range of Ti concentrations. I believe that the Bustee pyroxene-oldhamite clast reveals the solution to this problem. As outlined earlier in this paper, the oldhamite spherules may have formed upon cooling and crystallization of a silicate melt with dissolved CaS. As cooling proceeded, this CaS formed an immiscible sulfide melt and would have incorporated other chalcophile elements from the silicate melt (*e.g.*, Mn, Fe, Ti). Within this immiscible CaS melt, a second immiscible sulfide melt rich in iron formed. A number of works (*e.g.*, DICKINSON and MCCOY, 1997; this work) have demonstrated immiscibility in Fe-Ca-Mg-S melts. It is the occurrence of two immiscible sulfide melts which ultimately produces the Ti enrichment in FeS. Titanium is highly incompatible in oldhamite, as suggested both by the absence of Ti in the oldhamite of the pyroxene-oldhamite clast (Table 2) and the experimental Ti partition coefficient between FeS and CaS approaching infinity. Thus, FeS melt co-crystallizing with CaS melt or FeS exsolving from CaS would incorporate essentially all of the Ti from the system and could, in theory, become quite enriched in Ti.

The amount of enrichment of Ti in FeS co-existing with CaS depends on a number

of factors. The most important of these is the bulk Ti concentration of the sulfide melt and the relative proportions of FeS and CaS. For example, if we assume a CaS/FeS ratio of 100 (appropriate to the Bustee case) and bulk Ti concentration for the Ca-Fe-S melt of 0.2 wt%, we can produce a Ti concentration in troilite of 20 wt%. Thus, a small and realistic concentration of Ti in the bulk sulfide melt can produce the Ti-rich troilite observed in the Bustee pyroxene-oldhamite clast. Troilites within the Bustee pyroxene-oldhamite clast have a range of Ti concentrations (17.2–25.2 wt%) and several explanations exist for this range. The most obvious of these is that the individual oldhamite spherules within the clast are essentially isolated magmatic systems. As noted earlier, the range of Ti concentration within an individual oldhamite spherule is considerably less (≤2.3 wt%) than within the clast as a whole (8 wt%). A small range within an individual spherule is not unexpected, given that FeS within the Ti partitioning experiments exhibited a range of Ti concentrations (6.2–7.7 wt%). Further, troilite within the Bustee pyroxene-oldhamite clasts appears to be a mixture of crystallization and exsolution products, potentially producing an even broader range of compositions.

Finally, it is worth noting that co-crystallization with or exsolution of other phases with troilite may also produce Ti enrichments. The most important of these may be daubréelite, which is frequently observed as an exsolution phase in troilite and incorporates only very minor amounts of Ti (Table 2). Likewise, niningerite in the Bustee pyroxene-oldhamite clast contains undetectable Ti concentrations (Table 2) and, thus, co-crystallization of troilite and niningerite (or alabandite) would produce Ti enrichments in troilite. The partitioning of Ti within these systems (*e.g.*, Fe-Cr-S; Fe-Mg-S; Fe-Mn-S), however, has not been experimentally investigated.

Aubrites and enstatite chondrites appear to sample two parent bodies, as suggested by Keil (1989). However, arguments against a direct derivation of aubrites by melting of known enstatite chondrites are considerably weakened in the light of discovery of a mechanism for enriching aubritic troilite in Ti, thus eliminating one of the longest-standing objections. Other objections still exist, such as the presence of pigeonite in aubrites (Taylor *et al.*, 1988; Keil, 1989). It is possible that complex and as yet poorly understood exchange of elements between the complex sulfide-metal-silicate assemblage produced during melting of enstatite chondrites under highly reducing conditions may also play a role in the solution of these objections, as suggested by McCoy *et al.* (1997).

Acknowledgments

Monica Grady of The Natural History Museum generously provided invaluable access to and information about Bustee. This work benefited tremendously from a continuing collaboration with Tammy Dickinson and Gary Lofgren on experimental studies of enstatite meteorites. Encouragement by and discussions with Klaus Keil, Maya Wheelock and Ignacio Casanova in the early stages of this work are appreciated. Expert technical assistance with various aspects of this work was provided by the photographic unit of The Natural History Museum, Vincent Yang (JSC), Penny Bernhard (JSC), Tim O'Hearn (Smithsonian), Tim Gooding (Smithsonian) and Ben Hanson (JSC). Constructive comments by Drs. Tammy Dickinson, Sara Russell, Makoto Kimura and

Hiroko NAGAHARA substantially improved the manuscript. This work was supported, in part, by a National Research Council postdoctoral fellowship at Johnson Space Center and NASA Grant NAG5-4490 (TJM, P.I.).

References

BANNISTER, F.A. (1941): Osbornite, meteoritic titanium nitride. Mineral. Mag., **26**, 36–44.

BRETT, R. and KEIL, K. (1986): Enstatite chondrites and enstatite achondrites (aubrites) were not derived from the same parent body. Earth Planet. Sci. Lett., **81**, 1–6.

CASANOVA, I. (1992): Osbornite and the distribution of titanium in enstatite meteorites. Meteoritics, **27**, 208–209.

CHASE, M.W., DAVIES, C.A., DOWNING, J.R., FRURIP, D.J., MCDONALD, R.A. and SYVERUD, A.N. (1985): JANAF thermochemical tables. J. Phys. Chem. Ref. Data, **14, Suppl. 1.**

CLAYTON, R.N., MAYEDA, T.K. and RUBIN, A.E. (1984): Oxygen isotopic compositions of enstatite chondrites and aubrites. Proc. Lunar Planet. Sci. Conf., 15th, Pt. 1, C245–C249 (J. Geophys. Res., **89** Suppl.).

CROZAZ, G. and LUNDBERG, L.L. (1995): The origin of oldhamite in unequilibrated enstatite chondrites. Geochim. Cosmochim. Acta, **59**, 3817–3831.

DICKINSON, T.L. and LOFGREN, G.E. (1992): Melting relations for Indarch (EH4) under reducing conditions. Lunar and Planetary Science XXIII. Houston, Lunar Planet. Inst., 307–308.

DICKINSON, T.L. and MCCOY, T.J. (1997) Experimental rare-earth-element partitioning in aubrites: Implications for the igneous origin of aubritic oldhamite. Meteorit. Planet. Sci., **32**, 395–412.

FLIGHT, W. (1875): A chapter in the history of meteorites. Geol. Mag., **2**, 400–412.

FLIGHT, W. (1887): A Chapter in the History of Meteorites. London, Delau.

FLOSS, C. and CROZAZ, G. (1993): Heterogeneous REE patterns in oldhamite from the aubrites: Their nature and origin. Geochim. Cosmochim. Acta, **57**, 4039–4057.

FLOSS, C., STRAIT, M.M. and CROZAZ, G. (1990): Rare earth elements and the petrogenesis of aubrites. Geochim. Cosmochim. Acta, **54**, 3553–3558.

FOGEL, R.A. (1997): The enstatite chondrite-achondrite link reforged: Solution of the titanium in troilite problem. Meteorit. Planet. Sci., **32**, A43.

FOGEL, R.A., HESS, P.C. and RUTHERFORD, M.J. (1988): The enstatite chondrite-achondrite link. Lunar and Planetary Science XIX. Houston, Lunar Planet. Inst., 342–343.

FOGEL, R.A., WEISBERG, M.K. and PRINZ, M. (1996): The solubility of CaS in aubrite silicate melts. Lunar and Planetary Science XXVII. Houston, Lunar Planet. Inst., 371–372.

GROSSMAN, L. (1971): Condensation in the primitive solar nebula. Geochim. Cosmochim. Acta, **36**, 597–619.

KEIL, K. (1968): Mineralogical and chemical relationships among enstatite chondrites. J. Geophys. Res., **73**, 6945–6976.

KEIL, K. (1969): Titanium distribution in enstatite chondrites and achondrites, and its bearing on their origin. Earth Planet. Sci. Lett., **7**, 243–248.

KEIL, K. (1989): Enstatite meteorites and their parent bodies. Meteoritics, **24**, 195–208.

KEIL, K. and BRETT, R. (1974): Heideite, $(Fe,Cr)_{1+x}(Ti,Fe)_2S_4$, A new mineral in the Bustee enstatite achondrite. Am. Mineral., **59**, 465–470.

KEIL, K., NTAFLOS, Th., TAYLOR, G.J., BREARLEY, A.J., NEWSOM, H.E. and ROMIG, A.D., JR. (1989): The Shallowater aubrite: Evidence for origin by planetesimal impacts. Geochim. Cosmochim. Acta, **53**, 3291–3307.

KURAT, G., ZINNER, E. and BRANDSTÄTTER, F. (1992): An ion microprobe study of an unique oldhamite-pyroxenite fragment from the Bustee aubrite. Meteoritics, **27**, 246–247.

LODDERS, K. (1996a): Oldhamite in enstatite achondrites (aubrites). Proc. NIPR Symp. Antarct. Meteorites, **9**, 127–142.

LODDERS, K. (1996b): An experimental and theoretical study of rare-earth-element partitioning between sulfides (FeS, CaS) and silicate and applications to enstatite achondrites. Meteorit. Planet. Sci., **31**, 749–766.

LODDERS, K. and FEGLEY, B. (1992): Lanthanide and actinide condensation into oldhamite under reducing

conditions. Lunar and Planetary Science XXIII. Houston, Lunar Planet. Inst., 797–798.

McCoy, T.J., Dickinson, T.L. and Lofgren, G.E. (1997): Partial melting of Indarch (EH4) from 1000–1425°C: New insights into igneous processes in enstatite meteorites. Lunar and Planetary Science XXVIII. Houston, Lunar Planet. Inst., 903–904.

Nickel, E.H. and Mandarino, J.A. (1987): Procedures involving the IMA Commission on New Minerals and Mineral Names and guidelines on mineral nomenclature. Am. Mineral., **72**, 1031–1042.

Rubin, A.E., Scott, E.R.D. and Keil, K. (1997): Shock metamorphism of enstatite chondrites. Geochim. Cosmochim. Acta, **61**, 847–858.

Story-Maskelyne, N. (1870): On the mineral constituents of meteorites: The Busti aërolite of 1852. Philos. Trans. R. Soc. London, **160**, 189–214.

Taylor, G.J., Keil, K., Newsom, H. and Okada, A. (1988): Magmatism and impact on the aubrite parent body: Evidence from the Norton County enstatite achondrite. Lunar and Planetary Science XIX. Houston, Lunar Planet. Inst., 1185–1186.

Vogel, R. and Heumann, T. (1941): Das System Eisen-Eisensulfid-Kalziumsulfid. Archiv Eisenhüttenw., **15**, 195–199.

Watters, T.R. and Prinz, M. (1979): Aubrites: Their origin and relationship to enstatite chondrites. Proc. Lunar Planet. Sci. Conf., 10th, 1073–1093.

Wheelock, M.M., Keil, K., Floss, C., Taylor, G.J. and Crozaz, G. (1994): REE geochemistry of oldhamite-dominated clasts from the Norton County aubrite: Igneous origin of oldhamite. Geochim. Cosmochim. Acta, **58**, 449–458.

(Received August 18, 1997; Revised manuscript accepted December 18, 1997)